Solid State Sciences 175 (2026) 108249

Contents lists available at ScienceDirect

Solid State Sciences

journal homepage: www.elsevier.com/locate/ssscie

Solvothermal design of hierarchically interdigitated TiO_2 photoanodes with controlled nano-topology for efficient and scalable dye-sensitized solar cells

Syed Ezaz Haider Gilani [a], Khalil Harrabi [b,d], Rabia Nazar [a], Muhammad Farooq [a], Umer Mehmood [a,*], Muhammad Younas [c], Abdelkrim Mekki [b,e], Yong Zhang [f,**]

[a] Polymer and Process Engineering (PPE) Department, University of Engineering and Technology (UET), Lahore, Pakistan
[b] Department of Physics, College of Engineering and Physics, King Fahd University of Petroleum and Minerals (KFUPM), Saudi Arabia
[c] Core Research Facilities (CRF), KFUPM, PO Box 5047, Dhahran, 31261, Saudi Arabia
[d] Interdisciplinary Research Center for Intelligent Secure Systems, King Fahd University of Petroleum and Minerals, Saudi Arabia
[e] Interdisciplinary Research Center for Advanced Materials, King Fahd University of Petroleum and Minerals, Saudi Arabia
[f] School of Materials Science and Engineering, Harbin Institute of Technology, China

ARTICLE INFO

Keywords:
Interdigitated TiO_2
Nanorods
Charge transport
Photovoltaics
DSSC

ABSTRACT

The rational design of photosensitized solar cell (DSSCs) which is sensitive to improving the absorption of light, to transport the charges, and the stability of the structure is a key determinant to the development of the cell. This work describes the solvothermal synthesis of hierarchically interdigitated TiO_2 nanorod photoanodes with customized nanotopology, which are fabricated to maximize the movement of electrons and the ability to collect photons. The interdigitated architecture promotes directional charge transport, minimizes recombination losses, and significantly expands the active surface area for dye adsorption. XRD confirms the formation of nanorods with optimal crystallite size (~36.7 nm), reduced lattice strain, and favorable oxygen vacancy concentrations. SEM analysis revealed vertically aligned nanorods with uniform dispersion and optimal inter-rod spacing, facilitating efficient electrolyte penetration. TEM characterization further confirmed high aspect ratio (≈10:1), defect-free lattice fringes, and single-crystalline nature of the nanorods. XPS deconvolution indicated the presence of Ti^{3+} species and controlled oxygen vacancies, contributing to improved electronic conductivity and dye anchoring. Upon integration into DSSC devices, the solvothermally derived TiO_2 photoanodes yielded a power conversion efficiency (PCE) of 5.90%, representing a 20.6% enhancement over standard cells. The improvement is attributed to enhanced short-circuit current density (20.37 mA/cm^2), minimized series resistance (67.8 Ω), and optimized interfacial charge transfer resistance (147.2 Ω). These findings establish a direct structure–property–performance relationship, demonstrating that morphology-guided, defect-engineered TiO_2 architectures enable synergistic improvements in both photophysical and electrochemical behavior, providing a scalable platform for developing next-generation DSSCs with superior performance and stability.

1. Introduction

The demand on energy is growing at an alarming rate in the world because of the rapid industrialization, urbanization and the emergence of energy guzzling technologies. This scenario has led to the realization of the necessity of sustainable and renewable energy sources that will be able to offset the negative influence of environmental degradation and fossil fuel usage. Dye-sensitized solar cells (DSSC) have also gained great interest among the new photovoltaic materials due to low-cost processing, semi-transparent, flexible and potential performance in conditions of diffuse light [1,2]. DSSCs are an appealing field of creating new-generation energy harvesting technology, particularly in building-integrated photovoltaics and indoor IoT sensors, where the intensity of the light can fluctuate. However, as beneficial, at present, commercialization of DSSCs is restricted by their ability to transport charges, dye regeneration and photoanode instability.

One of the most important components of the DSSCs is the photoanode because it is a key component in determining the output of the device since it belongs to light collection, the dye adsorption process, and transmission of electrons into the conduction band. The most sought

---

* Corresponding author.
** Corresponding author.
E-mail addresses: umermehmood@uet.edu.pk (U. Mehmood), yongzhang@hit.edu.cn (Y. Zhang).

https://doi.org/10.1016/j.solidstatesciences.2026.108249
Received 26 October 2025; Received in revised form 25 January 2026; Accepted 2 February 2026

after photo anode material has been titanium dioxide (TiO_2), particularly rutile and anatase due to their suitable band alignment, high chemical stability, easy sourcing and non-toxicity [3,4]. This has seen the process of nanostructured TiO_2 photoanodes being identified as a significant method of enhancing the efficiency of the charge collection process by minimizing the diffusion length of the electrons and maximizing the contact area of the electrons with the dye molecules [5,6]. Morphological tuning via controlled synthesis pathways, including solvothermal, hydrothermal and electrospinning methods has been demonstrated to have a direct effect on the crystallinity, aspect ratio and porosity of TiO_2 nanostructures. The factors, in their turn, affect the rate of charge transport, recombination losses and, eventually, the power conversion efficiency (PCE) of DSSCs [7,8]. Nanostructures including nanorods and nanowires are one dimensional forms of TiO2 that offer a linear conduction route to transport the electrons, reducing scattering at the grain boundaries and maximizing the efficiency of charge loss to external contacts of the thin film [9].

DSSC has undergone a lot of research so as to enhance the efficiency of the device by optimizing the composition, morphology and structure of the photoanodes. Chandrika et al. [10] established the enhancement of PCE of both a gel-polymer electrolyte containing 17.5% TiO_2 nanoparticles to 7.30% with 28.1% improvement following the addition of the TiO_2 nanoparticles based on the increase in interfacial interactions and ionic conductivity. Dhulia and Yadav [11] synthesized nitrogen-doped TiO_2 materials and added them with the optimized ratios of azo dyes, which improved the charge separation and high PCE (0.349%) because of reduction in bandgaps. Similarly, Afzalina et al. [12] showed that the attenuation of the band gap to 2.4 eV and the improvement of light absorption and electron mobility after the addition of graphene to TiO_2 was observed. In an effort to improve the performance, Sonigara et al. [13] showed the application of anisotropic gel polymer electrolytes and modified TiO_2 photoanodes. Kathirvel et al. [14] effectively prepared TiO_2 nanorods by adopting the solvothermal method that showed improved dye adsorption and electron mobility as opposed to the electrodes made of the nanoparticles. Mao et al. [5] examined the photoelectrochemical characteristics of nanorods and nanotubes grown on conductive surfaces and discovered that vertically aligned nanorods presented better avenues of transporting electrons due to low recombination. Xu et al. [15] have addressed the stability issues of DSCs by substituting the liquid electrolytes with solid-state hole-transporting materials (HTMs). Despite stability improvements, solid-state DSCs (ss-DSCs) have shown lower efficiencies due to poor HTM infiltration in thick TiO_2 films. They overcame this by using multilayer TiO_2-coated ZnO nanowire arrays and a multistep HTM filling process, achieving an average efficiency of 5.65%. Uchida et al. [16] developed a simple one-step hydrothermal method to synthesize TiO_2 nanotubes (100 nm length, 8 nm diameter) with a high surface area of 270 m^2/g. However, DSSCs using these nanotubes achieved only 2.9% efficiency, lowr than that of TiO_2 nanoparticles. Li et al. [17] designed a double-layer TiO_2 (Ag–TiO_2-DL) photoanode combining P25 nanoparticles and 3D flower-like TiO_2 microstructures, with varying Ag nanoparticle loadings. At 0.8 wt% Ag, the DSSC achieved a high efficiency of 8.98% (vs. 6.22% without Ag), due to enhanced light harvesting, improved charge separation from hierarchical structures, and surface plasmon resonance of Ag nanoparticles. Brishty et al. [18] developed a flexible DSSC photoanode with forest-like TiO_2 hierarchical structures via a simple hydrothermal method, enhanced by Ag nanoparticles deposited through photoreduction. The branched TiO_2 enhanced dye loading, whereas Ag nanoparticles increased light absorption, scattering, and charge recombination. This structure showed a remarkable efficiency of 4.0%, surpassing pure nanowire and forest-like structures. Pandanga et al. [19] successfully prepared TiO_2 nanorods using a hydrothermal process with different TTIP ratios to optimize electron transport in DSSCs. The highest efficiency (0.08%) was obtained for a TTIP ratio of 2, due to the optimized nanorod structure that facilitated better dye adsorption and suppressed electron recombination. Vomiero et al. [20] successfully prepared TiO_2 nanotube arrays on flexible PET and Kapton HN substrates by anodization of titanium films. With N719 dye, flexible DSSCs showed a photoconversion efficiency of 3.5%. Chen et al. [21] designed double-wall TiO_2 nanotubes (DWTNTs) to address the low surface area of single-wall TiO_2 nanotubes (SWTNTs) in DSSCs. The DWTNTs, grown through a thoroughly described pore evolution process, showed enhanced dye adsorption and enhanced electron transport. Consequently, DSSCs with DWTNTs exhibited a higher efficiency of 6.90%, compared to 4.66% for SWTNTs.

In this research, a morphology-engineering strategy for improving the efficiency of DSSCs by designing interdigitated, hierarchically aligned TiO_2 nanorod photoanodes with a solvothermally synthesized method is introduced. In contrast to the traditional TiO_2 nanoparticle films, the interdigitated nanostructure designed in this research provides a synergistic improvement in light absorption and electron transport. The originality of this research is based on the integration of morphology engineering and experimental verification to provide a solid structure-property-performance correlation for future DSSCs. The results of this research are expected to fill the gap between computationally designed materials and the fabrication of high-efficiency solar cells.

2. Experimentation

2.1. Materials used

Analytical-grade titanium tetrachloride ($TiCl_4$) was obtained from Sigma-Aldrich. High-quality fluorine-doped tin oxide (FTO) glass substrates were obtained from Great-Cell Solar, Australia. The N3 dye, platinum paste, and ionic liquid electrolyte (Iodolyte Z-50) were obtained from Solaronix, Switzerland, ensuring the highest purity of materials for accurate experimental reproduction.

2.2. Fabrication and growth mechanism of interdigitated TiO_2 nanostructures

The interdigitated nanostructured TiO_2 photoanode was prepared using a solvothermal process to ensure high surface area, controlled morphology, and defined crystalline features for efficient dye-sensitized solar cell (DSSC) applications. A schematic representation of the preparation process is shown in Fig. 1. Fluorine-doped tin oxide (FTO) glass was used as the substrate material for TiO_2 growth. The precursor solution was prepared by dissolving titanium tetrachloride ($TiCl_4$) in a hydrochloric acid and deionized water mixture (1:2 v/v) under continuous stirring. Concentrations of different molarities (0.025 M, 0.05 M, and 0.075 M) were used to examine the influence of precursor concentration on nanostructure morphology. The synthesized solutions were loaded into a Teflon-lined autoclave, and the pretreated FTO substrates were immersed carefully to achieve oriented growth. The solvothermal reaction was performed at set temperatures of 160 °C, 180 °C, and 200 °C for different times (1, 3, and 5 h), which helped in the anisotropic growth of interdigitated nanostructures. After the solvothermal reaction, the TiO_2-coated FTO films were carefully taken out from the autoclave, washed thoroughly with deionized water to remove excess precursors, and dried in air. To enhance crystallinity, adhesion, and conductivity, the films were annealed at an optimal temperature of about 400 °C. A number of samples were synthesized by varying different synthesis conditions (temperature, time, and concentration) to optimize interdigitated nanostructured photoanodes.

The growth mechanism of rutile-phase TiO_2 nanorods by the hydrothermal method includes the controlled hydrolysis of $TiCl_4$ in an acidic aqueous solution. When $TiCl_4$ is added slowly to the water, it hydrolyzes to form titanium hydroxide as follows:

$$TiCl_4 + 4H_2O \rightarrow Ti(OH)_4 + 4HCl$$

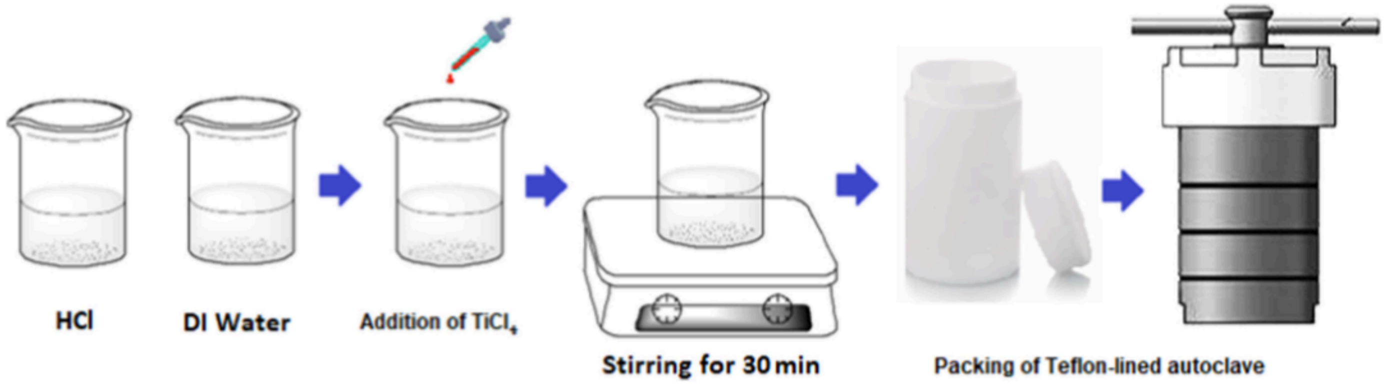

Fig. 1. Preparation of $TiCl_4$ precursor solution for solvothermal synthesis of TiO_2, followed by autoclave packing for hydrothermal treatment.

This exothermic step was carefully managed to avoid premature precipitation. The resulting $Ti(OH)_4$ species then undergo condensation:

$Ti(OH)_4 \rightarrow TiO_2$ (amorphous) + $2H_2O$

Under solvothermal conditions, the amorphous TiO_2 crystallizes into rutile-phase nanorods via oriented attachment, driven by acidic conditions that promote anisotropic growth:

TiO_2 (amorphous) → TiO_2 (rutile nanorods)

Hydrochloric acid is useful in the stabilization of Ti^{4+} ions and the anisotropic development of the crystal. The impact of this process is that vertically aligned rutile nanorods with high aspect ratio are formed, which is significant to present a high surface area as well as a continuous pathway of electron transport which are necessary to enhance light absorption and dye adsorption in DSSC photoanodes.

2.3. Fabrication of DSSCs

Photoanode preparation Photoanode was prepared as follows: N3 dye solution of 0.5 mM in methanol was prepared and the TiO_2 FTO substrates were immersed in the solution of dye, which is to be prepared in 24 h, to enable maximum dye adsorption. The electrodes were rinsed in ethanol after sensitization in order to clean them of any loosely adsorbed dye molecules. A platinum paste layer was prepared on a clean FTO substrate to create the counter electrode and to activate the catalytic property of the platinum surface, it was annealed at 450 °C over a period of 30 min. A sandwich assembly of the dye-sensitized photoanode and Pt counter electrode was then put together. Between the electrodes a liquid electrolyte (usually the I-/I3 - redox pair) was deposited via a capillary effect. The active area of the assembled DSSC was defined and fixed at a constant value of 0.2 cm^2 to ensure that photovoltaic characterization could be done concurrently.

2.4. Techniques and Instrumentation of characterization

X-ray diffraction (XRD) was used to examine the crystalline structure of interdigitated TiO_2 nanostructures (ultima IV, Riganaku, Japan). The surface morphology and nanostructure orientation that helped determine the dispersion, porosity, and general structure of the generated photoanodes were examined using scanning electron microscopy (SEM) (JSM-6610, JEOL, Japan). Transmission Electron Microscopy (TEM) (JEM-2100F, JEOL, Japan) was used to obtain the internal microstructure of TiO_2 nanorods. Additionally, the elemental composition was examined using the SEM system in conjunction with Energy Dispersive X-ray Spectroscopy (EDX) to demonstrate the existence and uniform distribution of oxygen and titanium. The Thermo-Scientific Escalab-250-Xi instrument was utilized to examine the oxidation state of cations and the chemical bonds between the elements using X-ray photoelectron spectroscopy. The material was studied using a monochromatic aluminum K-ray source with a power of 150 W and an energy of 1486.6 eV. The samples were exposed to radiation using an electron flood gun to counteract the charging effects. To determine the components included in the sample, a survey scan was obtained. At a pass energy of 20 eV, the O 1s, C 1s, Ti 2p, and Cl 1s high solution XPS spectra were captured. The adventitious C 1s at a BE of 284.8 eV was used to calibrate the binding energy (BE). Initially, the chamber's base pressure was 1×10^{-10} mbar "Avantage," a specialized software, was used to curve fit the core level spectra. Furthermore, Additionally, a solar simulator (MX-5, Solarphys Tech, USA) was used to assess the photovoltaic performance of the manufactured DSSCs under standard AM 1.5G illumination with an intensity of 100 mW/cm^2. Key device performance parameters, such as open-circuit voltage (V_{oc}), short-circuit current density (J_{sc}), fill factor (FF), and overall power conversion efficiency (PCE), were extracted using current-voltage (I–V) measurements.

3. Results & discussions

3.1. Scanning electron microscopy (SEM) analysis of TiO2 nanorods

To investigate the influence of precursor concentration on nanostructural evolution, TiO_2 films were synthesized using three different concentrations of $TiCl_4$: 0.025 M (sample-a), 0.05 M (sample-b), and 0.075 M (sample-c). The corresponding surface morphologies were examined using scanning electron microscopy (SEM), and the results are shown in Fig. 2. Sample-a (Fig. 2a & b) exhibits a highly uniform distribution of vertically aligned TiO_2 NRs with well-defined geometry and moderate porosity. The nanorods are ordered on the FTO surface with the estimated length being 1-2 μm and diameter being 50-100 nm. The distance between the rods is also sufficient regarding the ease with which it penetrates the electrolyte and the surfaces of the individual nanorods are highly smooth, a sign of high crystallinity and few surface defects. This morphology is the most preferable one in inhibiting the recombination of charge and enhancing the movement of electrons and the adsorption of dyes (Fig. 2a and b). Sample-b (Fig. 2c & d) on the contrary suggests agglomeration of the nanorods in which case, the agglomerated nanorods lose their alignment and porosity. This morphological defect is most likely to be because of improved nucleation rates and uncontrolled lateral development at elevated precursor concentrations. Sample-c (Fig. 2e and f) shows that a lot of coalescence of particles occurs and thus the films are high and compact and have low pore volume. These compact films are highly detrimental to electrolyte diffusion and interfacial contact with the dye molecules, potentially causing serious device performance degradation. These results are in line with the general observation that lower precursor concentrations are more conducive to anisotropic growth and morphological homogeneity, whereas higher concentrations are conducive to isotropic growth and particle aggregation, which are detrimental to functional properties.

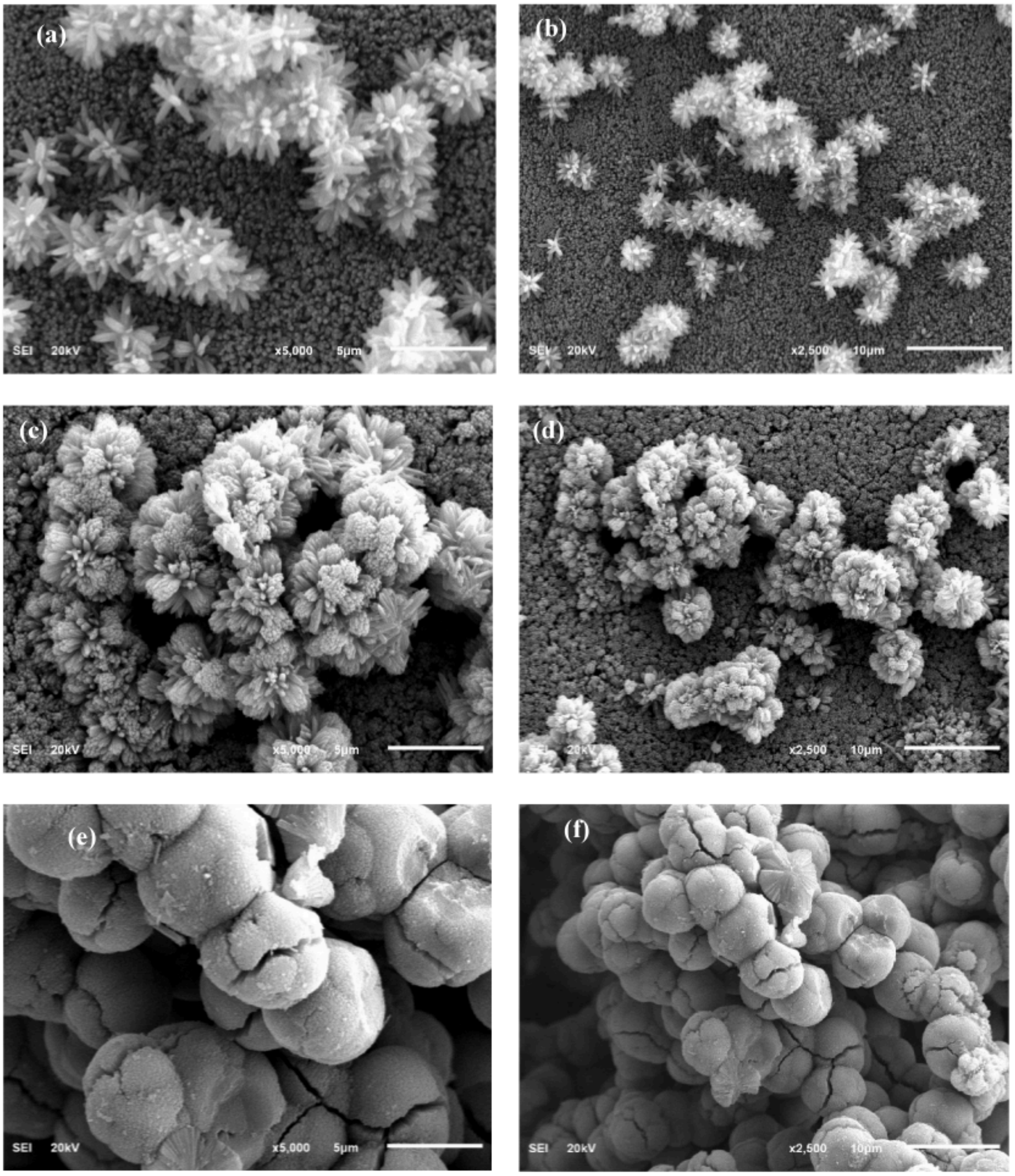

Fig. 2. SEM images of TiO_2 structures synthesized using different $TiCl_4$ precursor concentrations: (a & b) 0.025 M (sample-a), (c & d) 0.05 M (sample-b), and (e & f) 0.075 M (sample-c) at scale bars of 5 μm and 10 μm.

Of the three, sample-a has the most desirable set of structural properties such as vertical alignment (Fig. 3), porosity, and nanorod uniformity, which are critical for efficient DSSCs. The one-dimensional structure of TiO_2 NRs provides a straight route for electron transport, which is less prone to grain boundary scattering than nanoparticle films.

To explore the effect of thermal treatment on this optimal morphology, sample-a (0.025 M $TiCl_4$) was further subjected to solvothermal synthesis at three different temperatures: 160 °C (T1), 180 °C (T2), and 200 °C (T3). These samples were further characterized by XRD, TEM, and XPS to come up with a complex structure property performance relationship. How temperature affects crystallinity, strain and charge transport behavior is discussed in the following sections. 3.2. Analysis of TiO_2 Nanorods using X-ray Dispersion (XRD). Comparison of three samples T1, T2, and T3 prepared at 160 °C, 180 °C, and 200 °C with the help of 0.025 M $TiCl_4$ showed that significant changes in the crystallographic characteristics of samples which have direct impact on the efficiency of the devices occurred. It was determined that the solvothermal temperature can have a strong impact on the formation of crystallites and phases as seen in the XRD patterns (Fig. 4). All samples have diffraction peaks of the rutile phase of TiO_2 with the overwhelming reflections at 2θ 26.5deg, 36.2deg, 38.0deg, and 51.5deg indexed to the (110)-plane, (101)-plane, (004)-plane, and (211)-plane, respectively. These peaks prove the growth of rutile-phase TiO_2 with preferential orientations especially in that (004) plane in T2, which means there is vertical alignment of the nanorods. The crisp and clear peaks in T2 sample synthesized at 180 °C indicate better crystallinity than T1 and T3. Table 1 shows the size of the crystallites calculated as $D = Kl/b\cos\theta$ T1, T2 and T3 were found to have average crystallite sizes of 44.83 nm, 36.70 nm and 41.68 nm respectively. T1, prepared at 160 °C, had the highest mean crystallite size and the maximum number of peaks (FWHM range: 0.158deg-0.285deg) which implies that crystallization was not fully completed and that microstructural defects might be present. On the other hand, T2 had moderately sized crystallites (33.34-43.50 nm) and less FWHM (0.212deg-0.262deg) indicating better crystallization without grain enlargement. Though, T3, which was synthesized at 200 °C, was more crystalline than T1, the average crystallite size

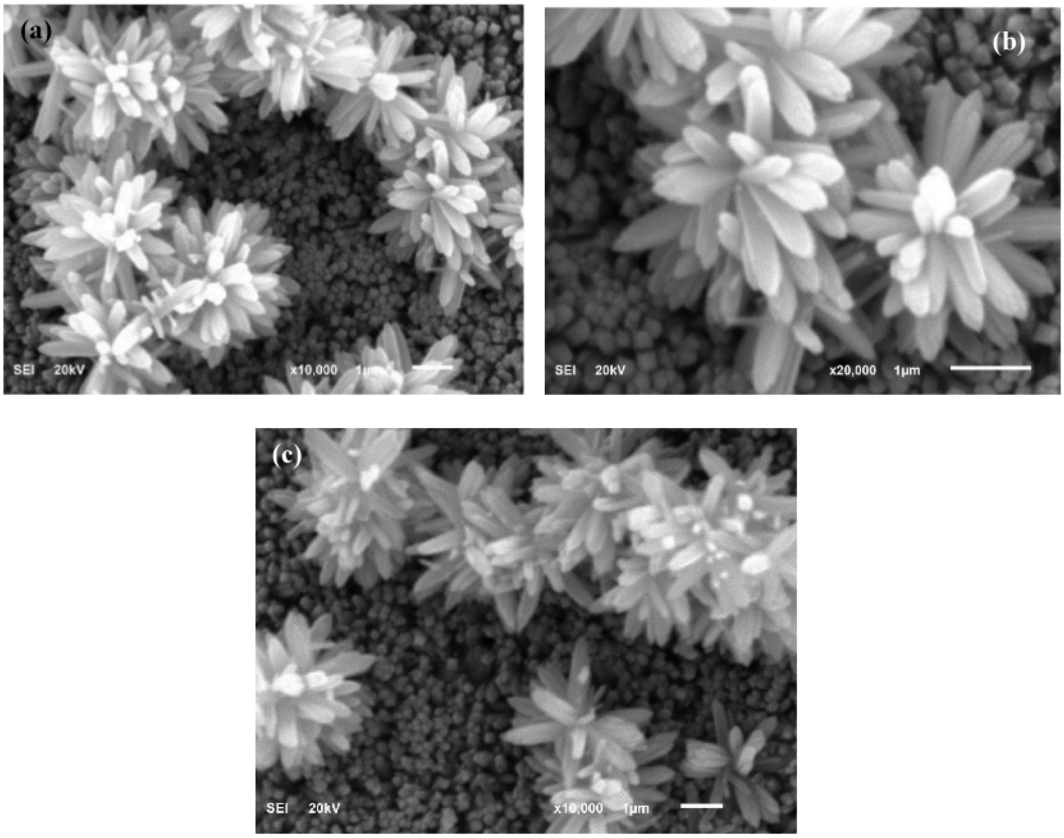

Fig. 3. SEM images of TiO_2 nanorods synthesized from 0.025 M $TiCl_4$ precursor.

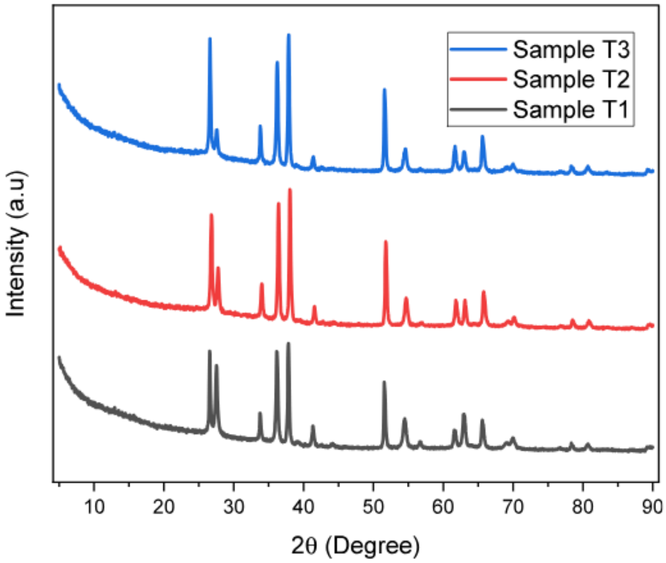

Fig. 4. XRD patterns of TiO_2 nanorods synthesized at different temperatures (T1: 160 °C, T2: 180 °C, T3: 200 °C), showing rutile-phase peaks with enhanced crystallinity in T2.

increased indicating the beginning of grain coalescence and this might decrease the effective surface area available to dye loading and also the mobility of electrons. In order to further study structural integrity, lattice strain (e) was obtained by means of the Williamson-Hall (W-H) technique (b cos th = kl/D+4e sinθ). The strain values (Table 1) obtained after the calculation show that T1 has the least lattice strain (~0.04209) due to poor annealing and causing imperfection in the lattice. T2 presents a little more strain (~0.04834), but it is evenly distributed, which is indicative of structural stability and enhanced charge transfer. The strain of T3 is intermediate (~0.044111), which may be explained by the fact that stress is created when T3 is synthesized because of the mismatch of thermal conditions. Notably, too much strain may result in defect states, which causes charge trapping and recombination. Surface morphology that is available in SEM images (Figs. 2 and 3) is in line with the structural data. The wider peaks and increased strain of T1 are also in accord with poorly defined morphology, with T3 exhibiting sintering and agglomeration at higher temperatures. T2 has a homogeneous and dispersed nanostructure, which is verified by SEM and XRD and structurally the most favorable one in high-efficiency DSSCs. The T2 peak T2 (004) with 100 percent relative intensity is further evidence of preferred orientation and well-aligned interdigitated TiO_2 nanorods which are essential conditions of effective electron transport and low recombination.

3.2. The characterization of TiO_2 nanorods by Transmission Electron Microscopy (TEM)

TEM micrographs of samples T1, T2 and T3 (Fig. 5) reveal obvious differences in the morphology of nanorods, which directly depend on the ability to load the dye, the movement of electrons and the rate of diffusion of the electrolytes. Sample T1, which was heated to 160 °C (Fig. 5a and b) is composed of irregularly-shaped nanorods with high levels of diameter variation (15-30 nm) and low aspect ratios (<8:1). The nanorods are very much kinked, bent and branched that would be hindrance to the electron transport channels hence, raising the transport resistance and rate of recombination. The chosen-area electron diffraction (SAED) pattern of the sample is composed of weak and disjointed rings, characteristic of the polycrystalline materials with random domains. T1 packing density too is uneven with localized aggregates of nanorods and probably decreases the available surface area to adsorb

Table 1
Crystallite size and lattice strain of TiO_2 nanostructures (T1, T2, T3) derived from XRD peak broadening using Scherrer's equation and lattice strain formula.

Sample	λ (Å)	2θ (°)	FWHM β (°)	D (nm)	θ (°)	cos θ	Lattice Strain (ε = β·cosθ/4)	Average D (nm)	Average ε
T1	0.15406	26.554	0.158	53.96	13.277	0.7580	0.02994	44.83	0.04209
		36.173	0.285	30.63	18.087	0.7227	0.05149		
		37.792	0.207	42.37	18.896	0.9989	0.05169		
		51.547	0.176	52.35	25.774	0.8016	0.03527		
T2	0.15406	26.794	0.252	33.85	13.397	0.6744	0.04249	36.70	0.04834
		36.389	0.262	33.34	18.195	0.7930	0.05194		
		38.012	0.243	36.11	19.006	0.9878	0.06001		
		51.758	0.212	43.50	25.879	0.7342	0.03891		
T3	0.15406	26.594	0.178	47.90	13.297	0.7448	0.03314	41.68	0.04411
		36.208	0.270	32.33	18.104	0.7347	0.04959		
		37.844	0.217	40.42	18.922	0.9974	0.05411		
		51.577	0.200	46.08	25.789	0.7926	0.03963		

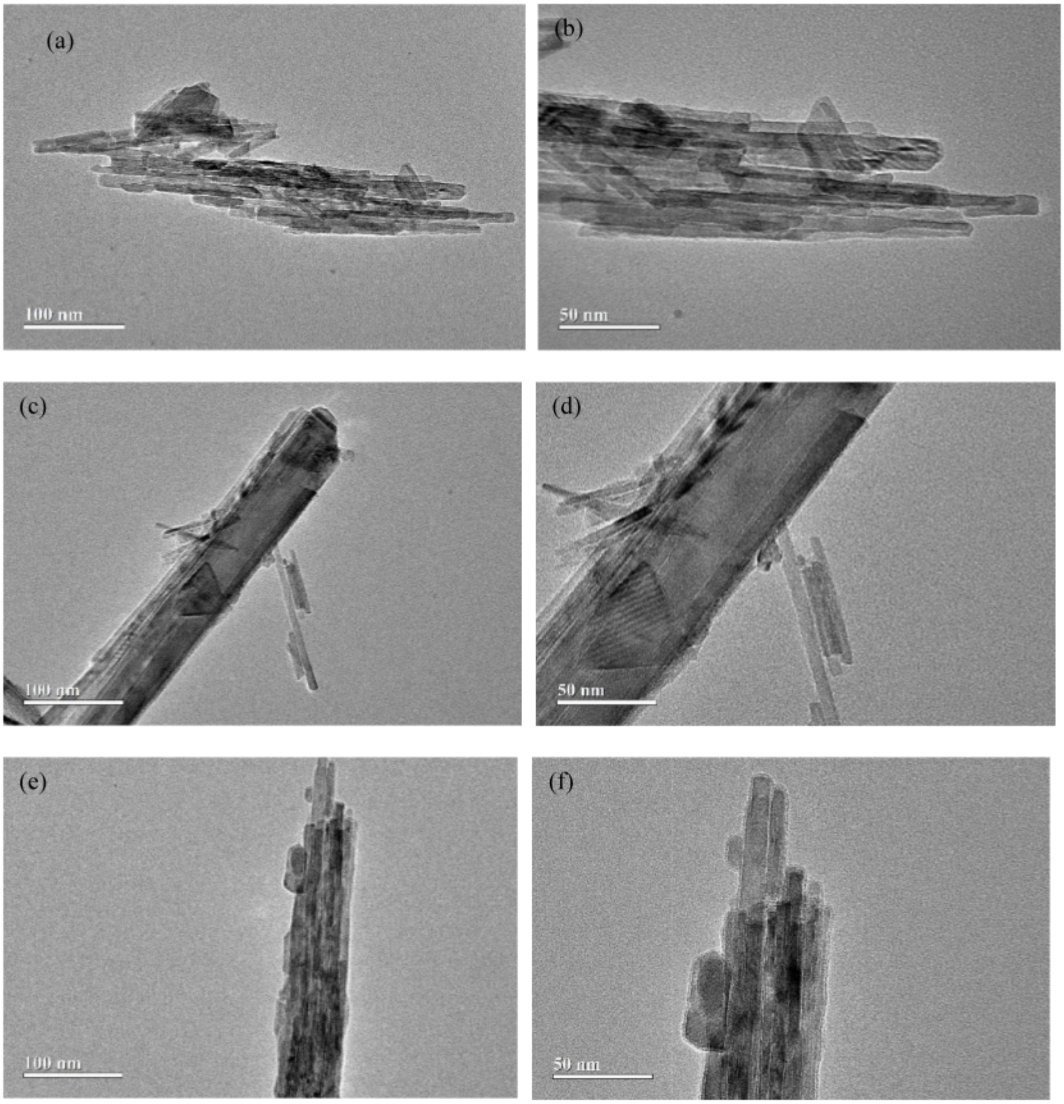

Fig. 5. TEM images of TiO_2 nanorods synthesized at varying solvothermal temperatures: (a & b) T1 (160 °C) showing irregular, kinked, low-aspect-ratio nanostructures; (c & d) T2 (180 °C) exhibiting uniform, high-aspect-ratio single-crystalline nanorods with inter-rod spacing of 5–7 nm; (e & f) T3 (200 °C) demonstrating coalesced, thickened nanorods with structural defects.

dye and blocks the infiltration of electrolytes. Similarly, Sample T2 (Fig. 5c and d), incubated at an optimum temperature of 180 °C, has much better morphology. The nanorods are straight, unbranched and highly aligned with uniform diameter of 20 +-2 nm with aspect ratio of more than 10:1. TEM images resolved by a lattice show clearly cut fringes separated by approximately 0.35 nm, which is the (110) plane of the rutile-phase TiO_2, and therefore indicates [001] growth direction. The SAED pattern exhibits high, sharp spots of the single-crystallinity and low structural defects. Rod to rod distances of 5-7 nm are recorded which is the optimum between high surface area to adsorb dyes and free passage of electrolytes. A combination of these properties facilitates high electron mobility, low recombination losses, and effective charge harvesting thus T2 is an excellent photoanode geometry to be used in DSSC. Sample T3, which was heated to 200 °C, shows a distinct evidence of structural degradation, as well as thermal coalescence. The numerous nanorods have fused together to produce bigger and broader (30-50 nm diameter) rods with reduced aspect ratios. It is also typical to neck between adjoining rods indicative of sintering phenomena that lower porosity and accessibility of surfaces. T3 SAED is mostly composed of spots and arcs implying partial crystallographic orientation loss (see Fig. 5e and f).

The SAED patterns also give an additional understanding of the crystal quality and the growth orientation of the TiO_2 nanorods synthesized under various solvothermal temperature. Fig. 5c-d demonstrates that the SAED pattern of sample T2 has sharp and well-rounded diffraction spots instead of rings, which is characteristic of a single-crystalline nature and preferred orientation of nanorods. The discrete spot pattern is consistent with rutile-phase TiO_2 and indicates coherent lattice ordering along the nanorod growth direction, in agreement with the lattice-resolved HRTEM fringes observed in Fig. 6c. In contrast, sample T1 displays diffuse and discontinuous diffraction rings, characteristics of polycrystalline domains and random crystallographic orientation, while sample T3 shows partial arcs resulting from thermal-induced coalescence and loss of structural coherence. These crystallographic differences have direct implications for charge transport behavior, as the single-crystalline nanorods in T2 provide uninterrupted electron pathways with minimal grain-boundary scattering, thereby suppressing recombination losses and facilitating efficient electron extraction in DSSC operation.

Further, TEM observation of sample T2 (Fig. 6) shows nanorods with a uniform length of approximately 188.5 nm and a diameter of 5-20 nm, which gives an aspect ratio of 9-19. This is very beneficial for DSSC applications, where the nanorods can facilitate directional electron transport along their length while providing enough surface area for dye adsorption. Fig. 6c presents a high-resolution TEM (HRTEM) image of a single TiO_2 nanorod from sample T2, clearly displaying well-defined lattice fringes, confirming its single-crystalline nature. The measured nanorod diameter is approximately 14.5 nm, which is consistent with earlier TEM observations and supports the narrow diameter distribution (5–20 nm) discussed in the analysis. The fringes are continuous, with no observable grain boundaries or dislocations, indicating minimal crystalline defects.

3.3. X-ray photoelectron spectroscopy (XPS) analysis of TiO_2 nanorods

XPS was utilized to characterize the structure and oxidation states of the cationic species within the three samples, T1, T2, and T3 investigated in this study. Fig. 7a shows the high-resolution Ti 2p spectra for the three samples revealing the usual $2p_{3/2}$ and $2p_{1/2}$ spin orbit splitting of the 2p level. The doublet spectrum for the T1 sample was wide, indicating multiple titanium species and therefore curve fitted with two peaks one at a binding energy (BE) of 458.66 eV and the other at a BE of 459.15 eV due to titanium in the Ti^{3+} and Ti^{4+} oxidation states, respectively. The proportion of Ti^{4+} is much smaller than that of Ti^{3+} as indicated by the small peak for Ti^{4+} contribution. The fitting resulted in 95% Ti^{3+} and the remaining 5% being Ti^{4+}. The spectrum for the T2 sample was found to be narrow and therefore was fitted with one contribution. The $2p_{3/2}$ peak is at a BE energy of 458.60 eV and assigned to titanium in Ti^{3+} oxidation state. Similar fitting was done for the Ti $2p_{3/2}$ of sample T3 and the fitting gave a BE of 258.64 eV and assigned to Ti^{3+} state. The results of the fitting are summarized in Table 1. The analysis of the Ti 2p spectra indicate that titanium exits predominantly in the Ti^{3+} oxidation state in the three samples. The Ti 2p core-level spectra further elucidate the oxidation states of titanium in the synthesized TiO_2 nanorods, as summarized quantitatively in Table 2. The doublet spectrum for sample T1 is relatively broad, indicating the coexistence of multiple titanium species. Accordingly, the Ti $2p_3/_2$ peak was curve-fitted with two contributions located at binding energies of 458.66 eV and 459.15 eV (Table 2), corresponding to Ti^{3+} and Ti^{4+} oxidation states, respectively. The dominance of the Ti^{3+} component reflects the presence of oxygen vacancies and reduced titanium species induced by lower-temperature synthesis. In contrast, the Ti 2p spectrum of sample T2 is narrower and can be fitted with a single dominant Ti^{3+} contribution at 458.60 eV (Table 2), indicating a more uniform chemical

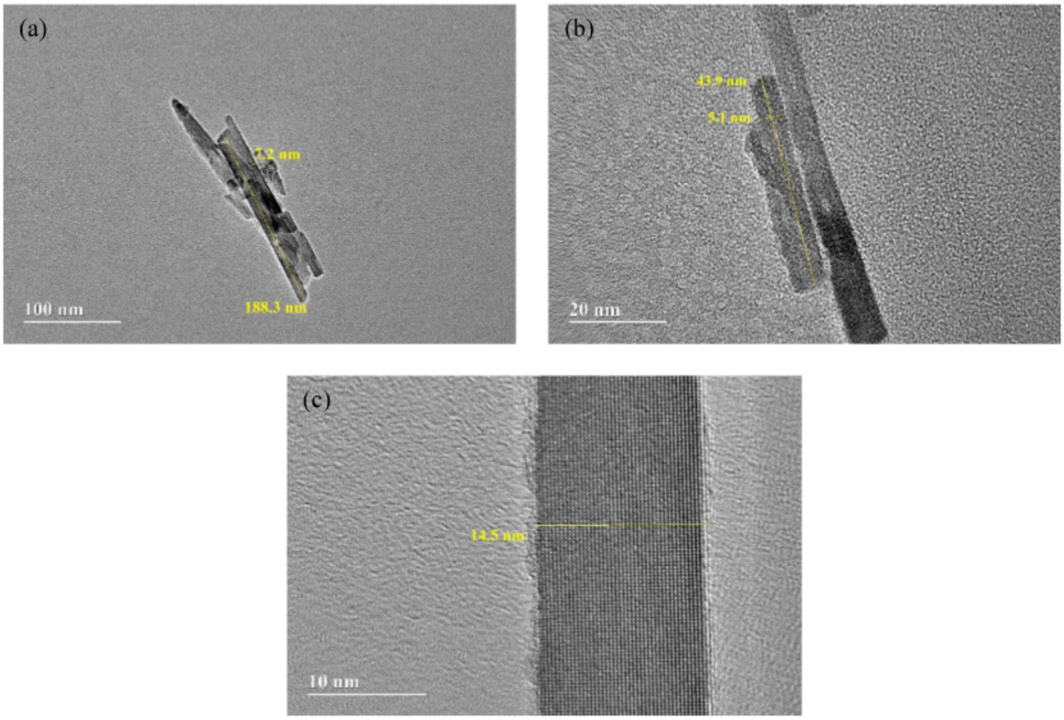

Fig. 6. High-resolution TEM image of TiO_2 nanorods (sample T2) showing (a & b) lengths of ~188.5 nm and diameters ranging from 5 to 20 nm, confirming high aspect ratio and single-crystalline structure and c) visible lattice fringes confirm crystallinity favorable for enhanced charge transport in DSSCs.

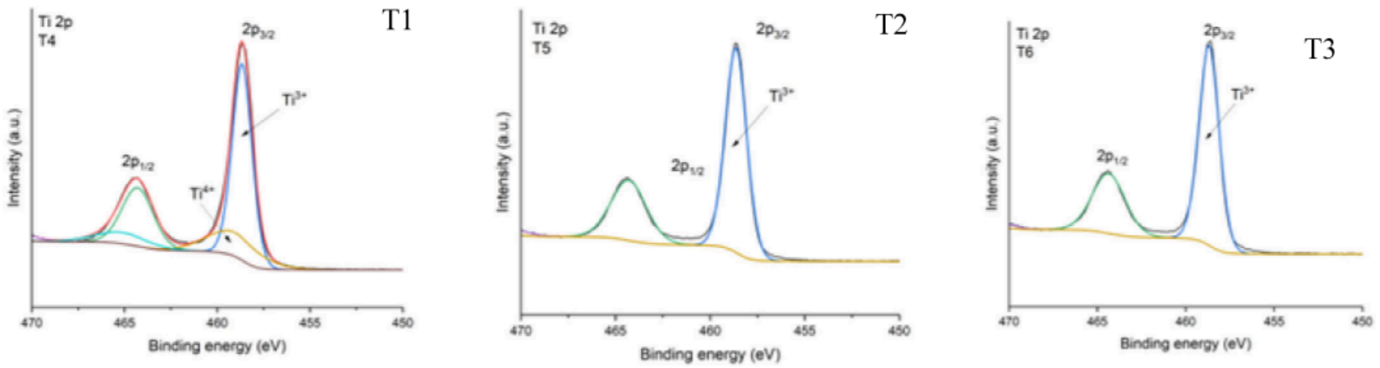

Fig. 7a. Fitting of Ti 2p core level spectra for the three samples (T1, T2, and T3).

Table 2
Results of the fitting of the Ti 2p, O 1s, Cl 2p core level spectra of TiO_2 nanorods samples.

Sample	BE (eV)	FWHM (eV)	BE (eV)	FWHM (eV)
	Ti 2p$_{3/2}$ **Ti^{3+}**		**Ti^{4+}**	
T1	458.66	1.25	459.15	3.3
T2	458.6	1.33	459.15	3.3
T3	458. 64	1.34	459.15	3.3
	Ti2p$_{1/2}$ **Ti^{3+}**		**Ti^{4+}**	
T1	464.33	1.25	465.15	3.3
T2	464.33	1.33	465.15	3.3
T3	464.40	1.34	465.15	3.3
	O 1s **O-Ti, O-Cl**		**O-H**	
T1	530.24	1.14	531.00	2.21
T2	530.11	1.28	531.49	2.93
T3	530.26	1.16	532.25	2.95
	Cl 2p$_{3/2}$		**Cl 2p$_{1/2}$**	
T1	198.7	3.17	200.4	3.17
T2	198.7	2.15	200.2	2.15
T3	198.7	2.15	200.2	2.15

environment and reduced surface disorder. Sample T3 shows a similar Ti^{3+}-dominated feature with a Ti $2p_3/_2$ peak centered at 458.64 eV (Table 2), suggesting preservation of reduced titanium states despite higher synthesis temperature.

The O 1s core level spectra for the three samples are shown in Fig. 7b. In all three cases the peaks are asymmetric and broad, indicating oxygen atoms exist in more than one coordination state. All three O 1s peaks were fitted with two contributions (summarized in Table 2), one due to lattice oxygen, i.e. O-Ti and O-Cl (in the case of samples T1 and T2) and it is the predominant contribution to the O 1s peak. The other smaller peak is assigned to oxygen vacancy-related defect states [22]. The peak energy of the lattice oxygen was found to be 530.2 eV, while the oxygen vacancy-related peak has a BE of approximately 531.2 eV (Table 2). In fact, the presence of Ti^{3+} indicates the presence of the oxygen vacancy [23,24].

According to the XPS analysis sample T3 did not contain chlorine as no Cl 2p contribution was detected. Fig. 7c displays Cl 2p core level spectra from samples T1 and T2. Both spectra were curve fitted with the usual $2p_{3/2}$ and $2p_{1/2}$ spin-orbit levels. The BE of the $2p_{3/2}$ peak was found to be 198.7 eV indicating this contribution is from Ti-Cl and/or O-Cl. The presence of residual chlorine was further confirmed by the Cl 2p spectra of samples T1 and T2, with fitted Cl $2p_3/_2$ peaks located at 198.7 eV and corresponding spin–orbit components listed in Table 2. The reduced FWHM and lower intensity of the Cl-related peaks in T2 compared to T1 indicate more effective removal of chloride species at the optimized synthesis temperature, while no detectable Cl signal was observed for T3 (Table 2), confirming chlorine-free surface chemistry at higher temperatures.

These findings align well with the structural observations from XRD and TEM, reinforcing the role of synthesis conditions in tuning the electronic properties of TiO_2 photoanodes.

3.4. *Current-voltage (I-V) characteristics of DSSCs*

The current–voltage (J–V) characteristics of DSSCs fabricated using TiO_2 nanorod photoanodes (T1, T2, and T3) and a standard TiO_2 electrode are presented in Fig. 8, with the key photovoltaic and electrical parameters summarized in Table 3. These parameters include power conversion efficiency (PCE), V_{oc}, J_{sc}, FF, series resistance (R_s), shunt

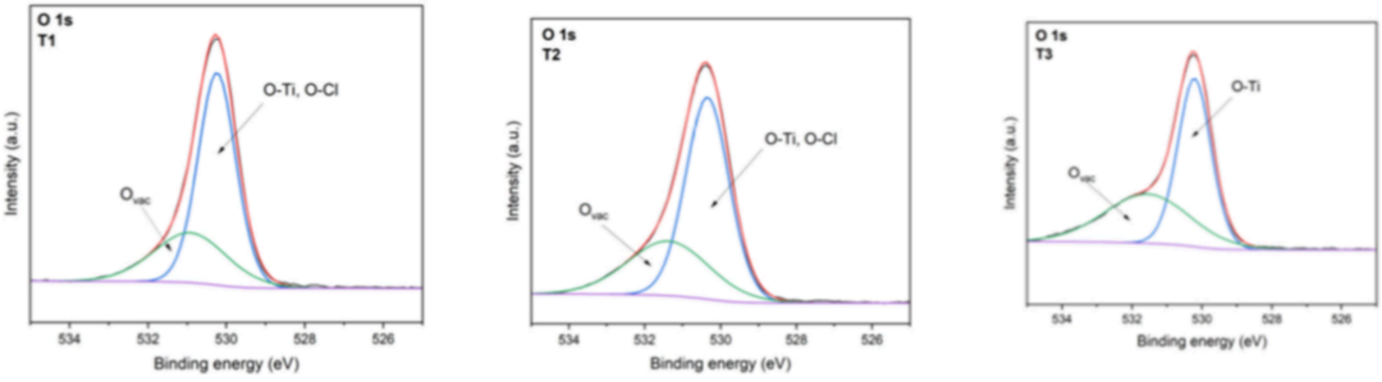

Fig. 7b. Fitting of the core level spectra for O 1s level for samples T1, T2 & T3.

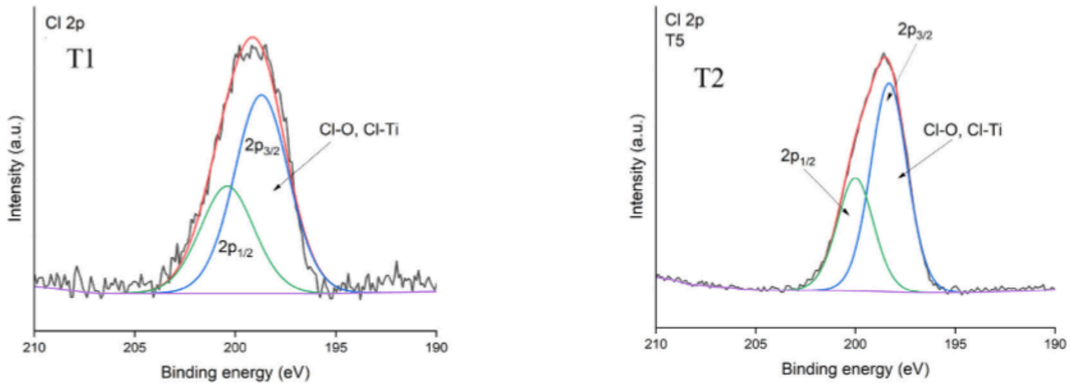

Fig. 7c. Fitting of the Cl 2p core level spectra for T1 and T2 samples.

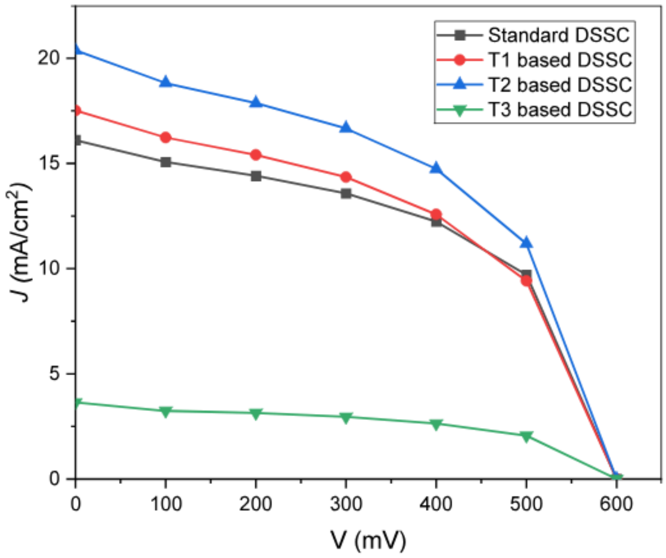

Fig. 8. Current–voltage (J–V) curves of DSSCs fabricated using standard TiO_2 and solvothermally synthesized TiO_2 nanorod photoanodes (samples T1, T2, T3).

resistance (R_{sh}), and charge transfer resistance (R_{ch}). The analysis provides a comprehensive understanding of how morphological and structural features impact device performance.

The baseline DSSC, with a commercial TiO_2 photoanode, gives PCE = 4.89%, Jsc = 16.11 mA/cm^2, and FF = 0.506. The Rs = 81.74 Ω and Rch = 186.27 Ω are higher than T2 but lower than T3, showing a reasonable level of balance without the benefit of nanorod optimization. These results clearly show that optimized nanostructures, as in T2, can greatly enhance the performance of a DSSC above that of normal electrodes.

Among all the devices, sample T2 shows the best photovoltaic property with the highest PCE of 5.90%, which is a remarkable improvement over the conventional DSSC (4.89%) and other test samples. This is mainly due to its high Jsc value of 20.37 mA/cm^2, which is a direct consequence of the highly aligned and high-aspect-ratio nanorods with low surface defects, as evidenced by TEM and SEM studies. The uniform distance between the nanorods (5-7 nm) ensures efficient electrolyte and dye diffusion, while its single-crystalline property, ascertained by SAED and HRTEM studies, ensures unimpeded electron transport. In addition, the series resistance (Rs = 67.83 Ω) of T2 is the lowest among all the samples. When the value of Rs is lower then it indicates that minimal resistance in the transparent FTO, photoanode and contact areas occurs and thus the transportation of charges in the cell will be enhanced. A higher shunt resistance (Rsh = 355.05 Ω) implies that fewer leakage currents occur, whereas a lower charge transfer resistance (Rch = 147.24 Ω) implies that the electron injection process of the dye into the TiO_2 conduction band occurs faster, and the redox species is replaced faster at the counter electrode. These electrical parameters are excellent interfacial kinetics and low recombination losses, which is in agreement with the high Jsc value and enhanced fill factor (FF = 0.482). Sample T1 that had been prepared at lower temperatures of 160 °C has moderate photovoltaic (PCE = 5.03) and Jsc = 17.52 mA/cm^2 that is a little higher than the standard cell. As its nanorods are being formed, the structures and crystallinity level of the latter are unaligned and moderate, which is shown in the broader XRD peaks and polycrystalline SAED patterns. The series resistance (Rs = 79.52 Ω) is greater than that of T2, which means that there is a greater resistance in TiO_2 layer and at the electrode interfaces. The charge transfer resistance (Rch = 171.25 Ω) is also high, indicating slower electron injection and higher recombination because of structural defects. The shunt resistance (Rsh = 404.69 Ω) is lower than that of the standard cell, indicating slightly higher parasitic leakage current. These combined effects cause a lower FF (0.478) and a moderate loss in overall efficiency compared to T2. For Sample T3, treated at the highest temperature (200 °C), there is a drastic loss in PCE (1.06%) and Jsc (3.64 mA/cm^2). Structural studies (SEM and TEM) showed that high temperatures cause nanorod merging and sintering, resulting in thicker nanorods, decreased surface area, and higher grain boundary and dislocation concentrations. These structural defects provide plenty of sites for recombination, which strongly impede electron transport. This effect is prominently manifested in its high series resistance (Rs = 378.95 Ω), strongly indicating high resistance to current flow in the cell. The charge transfer resistance (R_{ch} = 824.32 Ω) is also extremely high, pointing to poor electron injection kinetics and ineffective regeneration of the redox electrolyte. Although shunt resistance (R_{sh} = 1998.98 Ω) is high, usually associated with low leakage

Table 3
Photovoltaic performance parameters of DSSCs fabricated with standard TiO_2 and solvothermally synthesized TiO_2 nanorod photoanodes (T1, T2, T3).

DSSCs based on	PCE (%)	V_{oc} (mV)	J_{sc} (mA/cm^2)	FF	R_s (ohm)	R_{sh} (ohm)	R_{ch} (ohm)
Standard Cell	4.893	600	16.105	0.506	81.741	516.564	186.272
Sample-T1	5.030	600	17.517	0.478	79.518	404.688	171.254
Sample-T2	5.896	600	20.374	0.482	67.835	355.057	147.243
Sample-T3	1.055	600	3.639	0.483	378.951	1998.978	824.318

current—it is inconsequential here, as the major losses arise from internal transport and interfacial recombination, not leakage. The overall low FF (0.483) further reflects the poor current collection capability of the device.

4. Conclusion

In this study, interdigitated TiO_2 nanorod photoanodes were successfully synthesized via a controlled solvothermal method using varying precursor concentrations and reaction temperatures to optimize morphology, crystallinity, and electronic properties for dye-sensitized solar cell (DSSC) applications. Among the fabricated samples, the photoanode synthesized using 0.025 M $TiCl_4$ at 180 °C (Sample T2) exhibited superior structural and functional characteristics. SEM and TEM analyses confirmed the formation of vertically aligned, high-aspect-ratio nanorods with uniform distribution and optimal inter-rod spacing, facilitating enhanced dye loading and efficient electrolyte infiltration. The TEM images and SAED patterns at high resolutions supported the single-crystalline structure and growth direction along [001], which was efficient in decreasing the grain boundary effects on the recombination of charges. The XRD indicated that T2 had more crystallinity and less lattice strain whereas the XPS spectra established that the main Ti^{3+} species, low surface contamination and low chlorine residues are crucial in enhancing the movement of electrons. Moreover, the values of photovoltaic performance captured that T2-based DSSCs had the highest PCE of 5.90% which could be attributed to the maximum short-circuit current density (20.37 mA/cm^2), the lowest series resistance (67.83 Ω), and the lowest charge transfer resistance (147.24 Ω). Conversely, T1 exhibited moderate performance because of structural disorder, while T3 presented a dramatic efficiency drop owing to the thermal-induced nanorod coalescence and defects. This study provides the first direct evidence of the synthesis-architecture-performance relationship in solvothermally engineered TiO_2 nanostructures and confirms that accurate morphological and electronic optimization of TiO_2 nanostructures is essential for maximizing the efficiency of DSSCs. The findings also confirm the great potential of solvothermal engineering as a scalable method for the next-generation photoanode fabrication. Future studies will focus on the design of hybrid nanostructures and co-sensitization approaches to further boost light absorption and device durability.

CRediT authorship contribution statement

Syed Ezaz Haider Gilani: Resources, Formal analysis. **Khalil Harrabi:** Formal analysis. **Rabia Nazar:** Supervision, Formal analysis. **Muhammad Farooq:** Formal analysis. **Umer Mehmood:** Writing – review & editing, Supervision, Resources, Project administration, Methodology, Investigation, Funding acquisition, Formal analysis. **Muhammad Younas:** Formal analysis. **Abdelkrim Mekki:** Formal analysis. **Yong Zhang:** Writing – review & editing, Supervision, Formal analysis.

Funding

This work was supported by the CPEC8 project funded by HEC, Pakistan.

Declaration of competing interest

The authors declare the following financial interests/personal relationships which may be considered as potential competing interests: Umer Mehmood reports administrative support, equipment, drugs, or supplies, and writing assistance were provided by Bangladesh University of Engineering and Technology. Umer Mehmood reports financial support was provided by Higher Education Commission Pakistan. Umer Mehmood reports a relationship with University of Engineering and Technology that includes: employment. Umer Mehmood has patent pending to No. NA If there are other authors, they declare that they have no known competing financial interests or personal relationships that could have appeared to influence the work reported in this paper.

Acknowledgement

The authors gratefully acknowledge the financial support provided by the CPEC-8 project funded by HEC, Pakistan. The authors also extend their sincere thanks to PPE, UET Lahore, for providing essential research facilities. Additionally, the authors acknowledge KFUPM, Saudi Arabia, for providing testing facilities.

Appendix ASupplementary data

Supplementary data to this article can be found online at https://doi.org/10.1016/j.solidstatesciences.2026.108249.

Data availability

Data will be made available on request.

References

[1] Y.M. Hailu, J.-C. Jiang, Computational study on the interaction of iodide Electrolyte/Dye/TiO_2 interface in dye-sensitized solar cells, ECS Meet. Abstr. MA2022-02 (2022) 2502, https://doi.org/10.1149/MA2022-02602502MTGABS.

[2] K. Sharma, V. Sharma, S.S. Sharma, Dye-sensitized solar cells: fundamentals and Current status, Nanoscale Res. Lett. 13 (2018) 1–46, https://doi.org/10.1186/S11671-018-2760-6, 2018 131.

[3] P. Wang, S.M. Zakeeruddin, J.E. Moser, M.K. Nazeeruddin, T. Sekiguchi, M. Grätzel, A stable quasi-solid-state dye-sensitized solar cell with an amphiphilic ruthenium sensitizer and polymer gel electrolyte, Nat. Mater. 26 (2) (2003) 402–407, https://doi.org/10.1038/nmat904.

[4] M.S. Su'ait, M.Y.A. Rahman, A. Ahmad, Review on polymer electrolyte in dye-sensitized solar cells (DSSCs), Sol. Energy 115 (2015) 452–470, https://doi.org/10.1016/J.SOLENER.2015.02.043.

[5] A. Mao, K. Shin, J.K. Kim, D.H. Wang, G.Y. Han, J.H. Park, Controlled synthesis of vertically aligned hematite on conducting substrate for photoelectrochemical cells: nanorods versus nanotubes, ACS Appl. Mater. Interfaces 3 (2011) 1852–1858, https://doi.org/10.1021/AM200407T.

[6] S. Ding, C. Yang, J. Yuan, H. Li, X. Yuan, M. Li, An overview of the preparation and application of counter electrodes for DSSCs, RSC Adv. 13 (2023), https://doi.org/10.1039/d3ra00926b.

[7] J.R. Jennings, A. Ghicov, L.M. Peter, P. Schmuki, A.B. Walker, Dye-sensitized solar cells based on oriented TiO_2 nanotube arrays: transport, trapping, and transfer of electrons, J. Am. Chem. Soc. 130 (2008) 13364–13372, https://doi.org/10.1021/JA804852Z/SUPPL_FILE/JA804852Z_SI_001.PDF.

[8] B. Sarkar, N. Singhal, R. Goyal, A. Bordoloi, L.N. Sivakumar Konathala, U. Kumar, R. Bal, Morphology-controlled synthesis of TiO_2 nanostructures for environmental application, Catal. Commun. 74 (2016) 43–48, https://doi.org/10.1016/J.CATCOM.2015.10.035.

[9] J. Qu, C. Lai, One-Dimensional TiO_2 nanostructures as photoanodes for dye-sensitized solar cells, J. Nanomater. 2013 (2013) 762730, https://doi.org/10.1155/2013/762730.

[10] R.P. Chandrika, S.M.S. Gunathilaka, J.P. Liyanage, K. Wijayaratne, G.R.A. Kumara, N.G.A. Karunathilaka, L.A. DeSilva, T.M.W.J. Bandara, Effect of titanium dioxide nanofillers on the properties of gel-polymer electrolytes and power conversion efficiency of dye-sensitized solar cells, J. Solid State Electrochem. 29 (2024) 2581–2600, https://doi.org/10.1007/S10008-024-06169-X/FIGURES/11.

[11] V. Dhulia, S. Yadav, Enhanced efficiency of dye-sensitized solar cells using nitrogen-titanium dioxide composites and optimized Azo dye mixtures, Int. J. Sci. Res. Sci. Technol. 11 (2024) 410–414, https://doi.org/10.32628/IJSRST2411469.

[12] B. Afzalina, M.D. Nurhafizah, S. Razak, W.I. Nawawi, Effect of modified titanium dioxide photoanode and agarose gel electrolyte on electrochemical studies of dye-sensitized solar cell, Opt. Mater. 150 (2024) 115275, https://doi.org/10.1016/J.OPTMAT.2024.115275.

[13] K.K. Sonigara, J.V. Vaghasiya, H.K. Machhi, J. Prasad, A. Gibaud, S.S. Soni, Anisotropic one-dimensional aqueous polymer gel electrolyte for photoelectrochemical devices: improvement in hydrophobic "2-Dye/Electrolyte interface, ACS Appl. Energy Mater. 1 (2018) 3665–3673, https://doi.org/10.1021/ACSAEM.8B00444/SUPPL_FILE/AE8B00444_SI_001.PDF.

[14] S. Kathirvel, C. Su, Y.J. Shiao, Y.F. Lin, B.R. Chen, W.R. Li, Solvothermal synthesis of TiO_2 nanorods to enhance photovoltaic performance of dye-sensitized solar cells, Sol. Energy 132 (2016) 310–320, https://doi.org/10.1016/J.SOLENER.2016.03.025.

[15] C. Xu, J. Wu, U.V. Desai, D. Gao, High-efficiency solid-state dye-sensitized solar cells based on TiO_2-coated ZnO nanowire arrays, Nano Lett. 12 (2012) 2420–2424, https://doi.org/10.1021/NL3004144.

[16] S. Uchida, R. Chiba, M. Tomiha, N. Masaki, M. Shirai, Application of Titania nanotubes to a dye-sensitized solar cell, Electrochemistry 70 (2002) 418–420, https://doi.org/10.5796/ELECTROCHEMISTRY.70.418.

[17] L. Zhao, C. Zhong, Y. Wang, S. Wang, B. Dong, L. Wan, Ag nanoparticle-decorated 3D flower-like TiO_2 hierarchical microstructures composed of ultrathin nanosheets and enhanced photoelectrical conversion properties in dye-sensitized solar cells, J. Power Sources 292 (2015) 49–57, https://doi.org/10.1016/J.JPOWSOUR.2015.05.017.

[18] B.D. Choudhury, C. Lin, S.M.A.Z. Shawon, J. Soliz-Martinez, H. Huq, M.J. Uddin, A photoanode with hierarchical nanoforest TiO_2 structure and silver plasmonic nanoparticles for flexible dye sensitized solar cell, Sci. Rep. 11 (2021) 1–11, https://doi.org/10.1038/s41598-021-87123-z, 2021 111.

[19] D. Ben Jemia, M. Karyaoui, M.A. Wederni, al, J. Deng, M. Wang, J. Fang, F. Mohammadpour, M. Altomare, S. So, J.J. Pandanga, N.M. Nursam, N. Prastomo, Synthesis and application of TiO_2 nanorods as photo-anode in dye-sensitized solar cells, J. Phys. Conf. Ser. 1191 (2019) 012023, https://doi.org/10.1088/1742-6596/1191/1/012023.

[20] A. Vomiero, V. Galstyan, A. Braga, I. Concina, M. Brisotto, E. Bontempi, G. Sberveglieri, Flexible dye sensitized solar cells using TiO_2 nanotubes, Energy Environ. Sci. 4 (2011) 3408–3413, https://doi.org/10.1039/C0EE00485E.

[21] W.C. Chen, M.H. Yeh, L.Y. Lin, R. Vittal, K.C. Ho, Double-Wall TiO_2 nanotubes for dye-sensitized solar cells: a Study of growth mechanism, ACS Sustain. Chem. Eng. 6 (2018) 3907–3915, https://doi.org/10.1021/acssuschemeng.7b04250.

[22] S. Ghosh, G.G. Khan, S. Varma, K. Mandal, Influence of film thickness and oxygen partial pressure on cation-defect-induced intrinsic ferromagnetic behavior in luminescent p-Type Na-Doped ZnO thin films, ACS Appl. Mater. Interfaces 5 (2013) 2455–2461, https://doi.org/10.1021/AM302649R.

[23] R.T. Gao, L. Wang, Stable cocatalyst-free $BiVO_4$ photoanodes with passivated surface States for photocorrosion inhibition, Angew. Chemie - Int. Ed. 59 (2020) 23094–23099, https://doi.org/10.1002/ANIE.202010908;WGROUP:STRING:PUBLICATION.

[24] Y. Xin, J. Tian, X. Xiong, C. Wu, S.A.C. Carabineiro, X. Yang, Z. Chen, Y. Xia, Y. Jin, Enhanced photocatalytic efficiency through oxygen vacancy-driven molecular epitaxial growth of metal–organic frameworks on BiVO4, Adv. Mater. 37 (2025) 2417589, https://doi.org/10.1002/ADMA.202417589;REQUESTEDJOURNAL:JOURNAL:15214095;WGROUP:STRING:PUBLICATION.